cational Programs from the University of Wisconsin, Eau-Claire, Carnegie-Mellon University (Pittsburgh, PA) and Cumberland College (Kentucky), respectively. This work is in part supported by the Camille and Henry Dreyfus Foundation through a Teacher-Scholar Award to M.-H. Whangbo. The authors express their appreciation for computing time on the ER-Cray computer, made available to us by the DOE.

Supplementary Material Available: Tables of refined anisotropic thermal parameters for all non-hydrogen atoms, hydrogen atom fractional coordinates, least-squares planes through the ET molecules, the calculated H-atom positions and lists of observed and calculated structure factors for β-$(ET)_2ICl_2$ and β-$(ET)_2BrICl$ at 298 and 120 K (102 pages). Ordering information is given on any current masthead page.

Heat Capacity and Phase Transitions of the Mixed-Valence Compound $[Fe_3O(O_2CCH_3)_6(py)_3](py)$[1]

Michio Sorai,*† Kazutoshi Kaji,† David N. Hendrickson,*‡ and Seung M. Oh‡

Contribution from the Chemical Thermodynamics Laboratory, Faculty of Science, Osaka University, Toyonaka, Osaka 560, Japan, and the School of Chemical Sciences, University of Illinois, Urbana, Illinois 61801. *Received July 19, 1985*

Abstract: The heat capacity under constant pressure, C_p, of oxo-centered mixed-valence $[Fe_3O(O_2CCH_3)_6(py)_3](py)$ has been measured with an adiabatic calorimeter between 12 and 300 K. Four phase transitions were found to occur at 111.4, 112.0, 185.8, and 191.5 K. These transitions can be classified basically into two groups: one is a lower-temperature phase transition with two C_p peaks in the 111-112 K region and the other is a higher-temperature phase transition evolving from ~115 K to culminate in two C_p peaks in the 185-191 K region. The total enthalpy and entropy of these phase transitions were determined by estimating plausible normal heat capacities to give 4940 J mol^{-1} and (30.58 ± 0.83) J K^{-1} mol^{-1}, respectively. By comparing the present results with the ^{57}Fe Mössbauer spectroscopy and the X-ray structural work reported for this complex, it is concluded that these phase transitions are associated with the *intra*molecular electron transfer in the mixed-valence Fe_3O complexes and the orientational disordering of the pyridine solvate molecules about the crystallographic C_3 axis. DTA data for the solid solutions, $[Fe^{III}_2Fe^{II}_{1-x}Co^{II}_xO(O_2CCH_3)_6(py)_3](py)$, indicate that the phase transition having a C_p peak at 185.8 K is due to the orientational order-disorder phenomenon associated with the pyridine solvate molecules. The observed transition entropy is much larger than the value (R ln 3) expected to result from electronic delocalization in the $Fe^{III}_2Fe^{II}$ triads and the orientational disorder (R ln 3) about the C_3 axis of the pyridine solvate molecules. Two possibilities to account for the remaining entropy are discussed: one is associated with changes in the orbital degeneracy of the Fe(II) ion and the other is the rotation of the pyridine solvate molecules about their pseudo-C_6 axes.

A variety of transition-metal compounds are known to change their electronic states in the solid state as the result of a change in temperature. Among them, mixed-valence complexes form one class; other examples are spin-crossover complexes[6-8] and complexes exhibiting thermochromism.[9] These compounds often exhibit interesting phase-transition phenomena, in which the change in electronic states is strongly coupled with a change in their phonon systems.

The present compound, μ_3-oxo-tris(pyridine)hexakis(acetato)iron(II)-diiron(III)monopyridine, $[Fe_3O(OAc)_6(py)_3](py)$, is a typical example of a trinuclear, oxo-centered mixed-valence iron acetate complex. Variable-temperature ^{57}Fe Mössbauer spectroscopy[10,11] for this compound has revealed interesting features characteristic of an *intra*molecular electron transfer, and suggesting a phase transition between the electron-localized and -delocalized states. Preliminary X-ray structural work[12] showed that $[Fe_3O(OAc)_6(py)_3](py)$ crystallizes in the space group $R32$ at room temperature, where there are stacks of Fe_3O complexes with a C_3 axis running down each stack. Recent ongoing X-ray structural work[13] shows that the pyridine solvate molecules, which have their molecular planes oriented perpendicular to the Fe_3O planes, are orientationally disordered in three positions about the C_3 axis at room temperature, whereas this symmetry axis disappears at low temperatures. On the basis of these experiments, two of the present authors and their collaborators[10,11] have emphasized the importance of a significant coupling between the motional state of the pyridine solvate molecule and the *intra*molecular electron-transfer rate in the Fe_3O complex.

Thermodynamic studies, in particular heat capacity measurements, serve as a powerful tool to elucidate energetic and entropic aspects of a phenomenon, from which one can obtain definitive evidence as to whether a phase transition exists or not. Moreover, based on the transition entropy, it is possible to discover microscopic processes which are involved in a phase transition that spectroscopic and structural studies fail to detect. One of the objectives of the present paper is to combine macroscopic entropic aspects complementarily with the microscopic aspects derived from spectroscopic and structural data. To this end, heat capacity measurements were made in the range from 12 to 300 K for $[Fe_3O(OAc)_6(py)_3](py)$. It will be shown that there are four phase

†Osaka University.
‡University of Illinois.

(1) Contribution No. 90 from the Chemical Thermodynamics Laboratory.
(2) Day, P *Int. Rev. Phys. Chem.* **1981**, *1*, 149.
(3) "Mixed-Valence Compounds: Theory and Applications in Chemistry, Physics, Geology and Biology"; Brown, D. B., Ed.; D. Reidel: New York, 1980.
(4) Creutz, C. *Prog. Inorg. Chem.* **1983**, *30*, 1.
(5) Richardson, D. E.; Taube, H. *Coord. Chem. Rev.* **1984**, *60*, 107.
(6) König, E. *Ber. Bunsenges. Phys. Chem.* **1972**, *76*, 975.
(7) Goodwin, H. A. *Coord. Chem. Rev.* **1976**, *18*, 293.
(8) Gütlich, P. *Struct. Bonding* **1981**, *44*, 83.
(9) Day, J. H. *Chem. Rev.* **1963**, *63*, 65.
(10) Oh, S. M.; Hendrickson, D. N.; Hassett, K. L.; Davis, R. E. *J. Am. Chem. Soc.* **1984**, *106*, 7984.
(11) Oh, S. M.; Hendrickson, D. N.; Hassett, K. L.; Davis, R. E. *J. Am. Chem. Soc.*, in press.
(12) See Table III in: Catterick, J.; Thornton, P. *Adv. Inorg. Chem. Radiochem.* **1977**, *20*, 291. Where it is indicated that $[Fe_3O(OAc)_6(py)_3](py)$ is isostructural to the analogous manganese compound, the structure of which has been communicated: Baikie, A. R. E.; Hursthouse, M. B.; New, D. B.; Thornton, P. *J. Chem. Soc., Chem. Commun.* **1978**, 62.
(13) Strouse, C. E.; Hendrickson, D. N.; Oh, S. M., unpublished results.

0002-7863/86/1508-0702$01.50/0

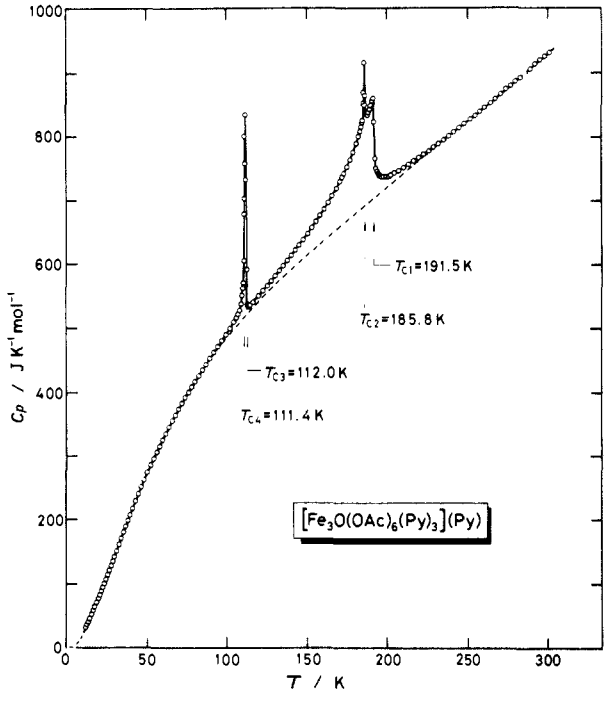

Figure 1. Molar heat capacity of $[Fe_3O(OAc)_6(py)_3](py)$. Broken line indicates the normal heat capacity curve.

transitions. The nature of these transitions, especially the degrees of freedom relevant to them, will be discussed. A part of the present results has been briefly reported elsewhere.[14]

Experimental Section

Sample Preparation. The preparation methods for $[Fe_3O(OAc)_6(py)_3](py)$ and $[Fe_2CoO(OAc)_6(py)_3](py)$ have been described previously.[11] The solid solutions, $[Fe^{III}_2Fe^{II}_{1-x}Co^{II}_xO(OAc)_6(py)_3](py)$ (x = 0.05, 0.20, 0.33, 0.50, and 0.60), were prepared by dissolving appropriate amounts of the Fe_3O and Fe_2CoO complexes in pyridine under an argon atmosphere. Evaporation of these solutions gave microcrystalline samples.

Differential Thermal Analysis (DTA). Preliminary observation of the thermal properties was made with a home-built DTA apparatus which operates between 60 and 530 K. The mass of a compound used for a probe in each case was about 300 mg.

Heat Capacity Measurements. Heat capacities were measured with an adiabatic calorimeter[15] from 12 to 300 K. A calorimeter cell[16] made of gold-plated copper was loaded with 17.7794 g (or 0.020 813 75 mol) of polycrystalline $[Fe_3O(OAc)_6(py)_3](py)$ with buoyancy correction assuming the density of 1.4 g cm^{-3}. A small amount of helium gas was sealed in the cell to aid the heat transfer.

Infrared Absorption Spectra. Variable-temperature IR spectra were recorded for Nujol mulls between 93 and 299 K with an infrared spectrophotometer Model DS-402G (Japan Spectroscopic Co., Ltd.) in the range 4000–400 cm^{-1} and with a far-infrared spectrophotometer Model FIS-3 (Hitachi, Ltd.) in the range 400–30 cm^{-1}.

Results

A DTA run for $[Fe_3O(OAc)_6(py)_3](py)$ exhibited four thermal anomalies at 191.6, 184.6, 109.2, and 108.0 K on cooling and three peaks at 110.7, 185.0, and 191.6 K on heating. The two lowest-temperature peaks of the cooling run are merged into a single peak at 110.7 K in the heating run. All the peaks, except the highest-temperature one, showed a small but significant thermal hysteresis, which indicates that these phase transitions involve a first-order character. In order to avoid the undercooling phenomenon characteristic of a first-order phase transition, the specimen in the adiabatic calorimeter was cooled quite slowly,

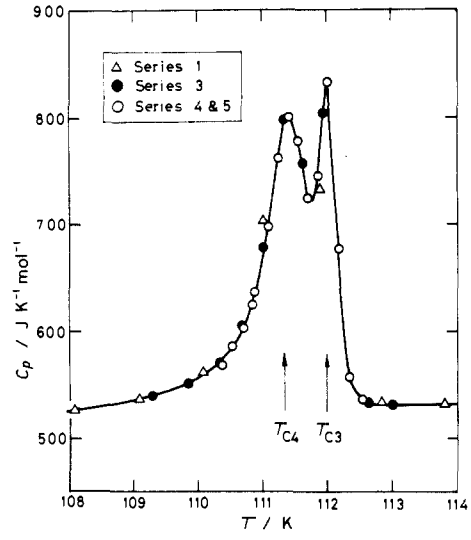

Figure 2. Molar heat capacity of $[Fe_3O(OAc)_6(py)_3](py)$ in the vicinity of the phase transitions at T_{C4} and T_{C3}.

especially when its temperature passed through the particular phase-transition points.

Calorimetric measurements were made in six series, the results of which were evaluated in terms of C_p, the molar heat capacity under constant pressure. The experimental data are listed in Table I and plotted in Figure 1. The four thermal anomalies detected by DTA were clearly observed by the heat capacity measurements as phase transitions at 111.4, 112.0, 185.8, and 191.5 K. These transition points will be henceforth designated as T_{C4}, T_{C3}, T_{C2}, and T_{C1}, respectively. Since the transitions at T_{C4} and T_{C3} successively occur in a narrow temperature interval, the heat capacities in this region are plotted as an inset in Figure 2 with an expanded scale of temperature.

Thermal relaxation time, the time required for thermal equilibration in the specimen after an electric-energy input to the calorimeter cell, was shorter than 15 min in the normal temperature region where there is no effect on a phase transition and even in the vicinity of T_{C1}, while it was elongated to 60 min or longer near T_{C4} and T_{C3} and to 30 min or longer near T_{C2}. The long thermal relaxation time also supports the first-order nature of the transitions at T_{C4}, T_{C3}, and T_{C2}. The long C_p tail spreading over ~115–190 K indicates that the transition at T_{C1} is of higher-order, a fact that is in agreement with the short thermal relaxation time and absence of thermal hysteresis observed for the phase transition at T_{C1}.

As can be seen in Figure 1, the four phase transitions can be classified basically into two groups: One is a lower-temperature phase transition with two C_p peaks at T_{C4} and T_{C3} and the other is a higher-temperature phase transition evolving from ~115 K to culminate in two C_p peaks at T_{C2} and T_{C1}. Variable-temperature ^{57}Fe Mössbauer spectra[10,11] for $[Fe_3O(OAc)_6(py)_3](py)$ show two quadrupole-split doublets below ~100 K, one characteristic of high-spin Fe^{II} and the other of high-spin Fe^{III}. As the sample temperature is increased, the first appreciable change in the spectrum is seen at ~117 K, where a third doublet appears. The spectrum changes dramatically as the temperature is further increased, eventually to become a single doublet above ~190 K, indicating that the rate of intramolecular electron transfer exceeds the ~10^7–10^8 s^{-1} rate which the Mössbauer technique can sense. It is of great interest that the LT-phase transition takes place at the temperature where the first Mössbauer spectrum change occurs and that the peak temperature of the HT-phase transition is identical with the temperature where the Mössbauer spectrum becomes a single average doublet. Moreover, the large temperature range involved in the HT-phase transition fully overlaps with the temperature region where the drastic change in the Mössbauer spectrum is occurring.

In addition to the *intra*molecular electron transfer, there is in the solid state of $[Fe_3O(OAc)_6(py)_3](py)$ an orientational or-

(14) Oh, S. M.; Kambara, T.; Hendrickson, D. N.; Sorai, M.; Kaji, K.; Woehler, S. E.; Wittebort, R. J. *J. Am. Chem. Soc.* **1985**, *107*, 5541.
(15) Construction of an adiabatic calorimeter workable between 12 and 530 K: Sorai, M.; Kaji, K., unpublished.
(16) Ogasahara, K.; Sorai, M.; Suga, H. *Mol. Cryst. Liq. Cryst.* **1980**, *71*, 189.

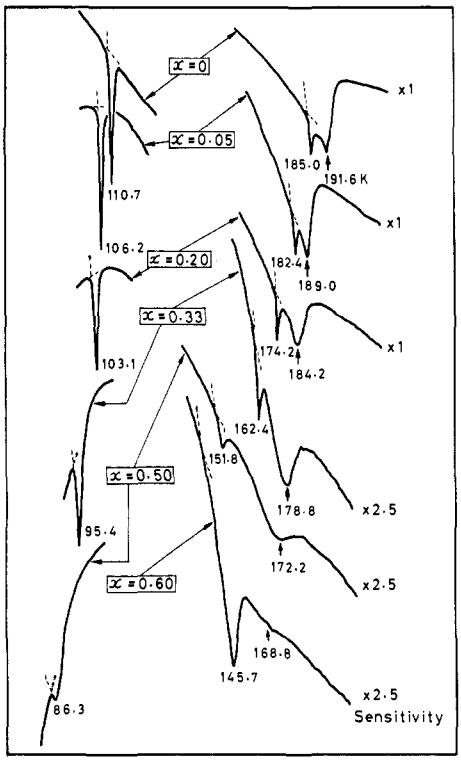

Figure 3. Heating runs of DTA for the solid solutions, $[Fe^{III}_2Fe^{II}_{1-x}Co^{II}_xO(OAc)_6(py)_3](py)$.

der–disorder transformation associated with the pyridine solvate molecules. Single-crystal X-ray diffraction work[13] indicates that the pyridine solvate molecules are sandwiched between the Fe_3O complexes in stacks and are disordered in three positions about a C_3 axis at room temperature. However, the C_3 axis disappears at ~190 K as the crystal is cooled from 300 K. In order to get more insight as to the relationship between the phase transitions and the order–disorder phenomenon of the pyridine solvate molecules, DTA measurements were made for the solid solutions of the present complex with isostructural $[Fe^{III}_2Co^{II}O(OAc)_6(py)_3](py)$ which obviously does not exhibit *intra*molecular electron transfer.[11] The results of the heating DTA runs for $[Fe^{III}_2Fe^{II}_{1-x}Co^{II}_xO(OAc)_6(py)_3](py)$ (x = 0.0, 0.05, 0.20, 0.33, 0.50, and 0.60) are reproduced in Figure 3. One of the remarkable features is that the intensities of the T_{C1} and T_{C3} peaks diminish with increasing x, whereas the intensity of the T_{C2} peak seems to remain unchanged. We can, therefore, conclude that the T_{C2} phase transition might be associated with the orientational order–disorder of the pyridine solvate molecules. A mystery, however, is why a DTA run of the pure Co complex (the x = 1.0 probe) did not show the "T_{C2}" peak. The reason seems to be its large thermal hysteresis. The hysteresis of this phase transition becomes larger with increasing x. For example, the x = 0 probe showed a peak at T_{C2} = 184.6 K on cooling and at T_{C2} = 185.0 K on heating, while in the case of the x = 0.50 probe T_{C2} occurred at 136.0 and 151.8 K for the cooling and heating runs, respectively. The lowest-temperature limit available for the present DTA apparatus (~60 K) is higher than the lower limit temperature of the thermal hysteresis for the x = 1.0 compound, and as a consequence, the failure to detect the "T_{C2}" is understandable.

Another interesting feature is the concentration dependence of the critical temperatures. As shown in Figure 4, all three phase-transition points are linearly shifted to lower temperatures with increasing x as if there is no critical concentration above which the phase transition disappears. Least-squares fitting the data gave the following relationships:

$$T_{C1}(x)/K = 191.4 - 37.7x$$

$$T_{C2}(x)/K = 185.7 - 66.9x$$

$$T_{C3}(x)/K = 110.3 - 46.1x$$

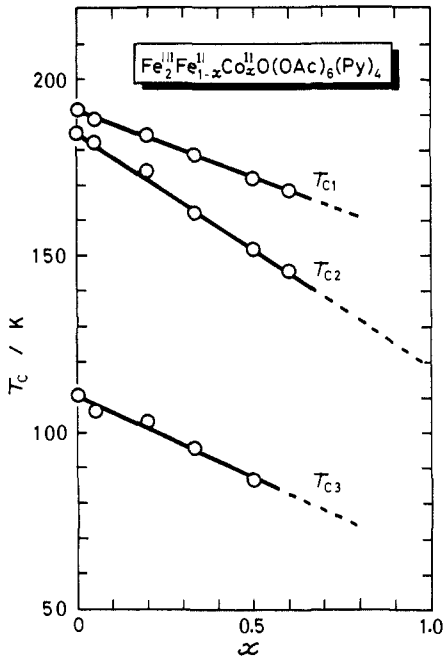

Figure 4. Concentration dependence of the transition points for the solid solutions, $[Fe^{III}_2Fe^{II}_{1-x}Co^{II}_xO(OAc)_6(py)_3](py)$.

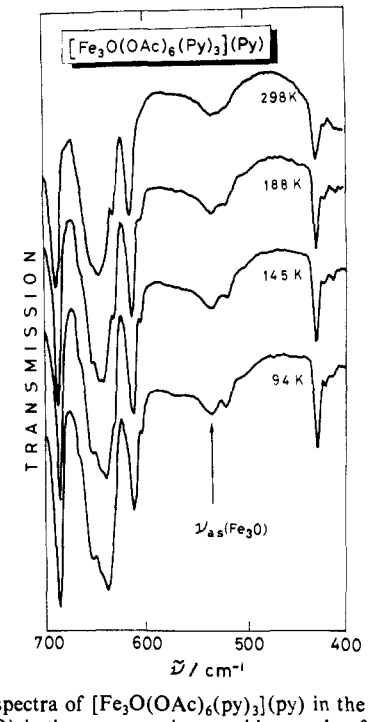

Figure 5. IR spectra of $[Fe_3O(OAc)_6(py)_3](py)$ in the range 700–400 cm^{-1}. $\nu_{as}(Fe_3O)$ is the asymmetric stretching mode of the Fe_3O core.

Thermodynamic Quantities Associated with Phase Transitions

To estimate the excess heat capacities due to the four phase transitions from the experimental values, it is necessary to estimate a "normal" heat capacity curve. To this end, an effective frequency distribution method[17] was employed. Since IR and/or Raman spectra are necessary for this method, IR spectra of $[Fe_3O(OAc)_6(py)_3](py)$ were recorded in the range 4000–30 cm^{-1} as a function of temperature. The IR spectra in the range 700–100 cm^{-1} are reproduced in Figures 5 and 6. Although the absorption bands in this wavenumber region are sensitive to changes in bond lengths, there exists no appreciable temperature dependence even if we compare the spectra of the highest-temperature electron-delocalized phase with those of the lowest-temperature electron-

(17) Sorai, M.; Seki, S. *J. Phys. Soc. Jpn.* **1972**, *32*, 382.

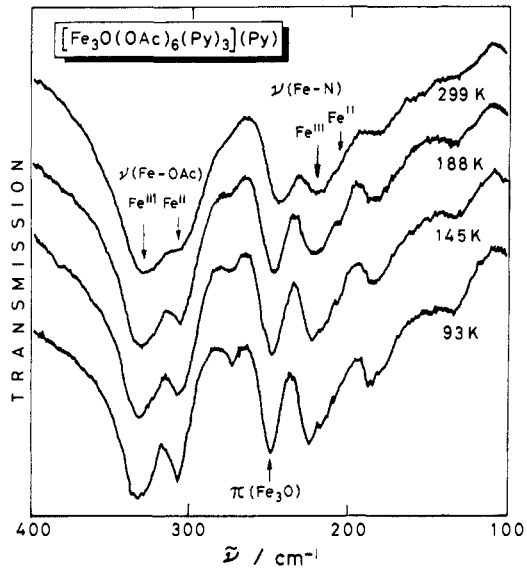

Figure 6. Far-IR spectra of $[Fe_3O(OAc)_6(py)_3](py)$ in the range 400–100 cm^{-1}. ν(Fe–OAc) and $\pi(Fe_3O)$ are the stretching modes between Fe and O (in acetate) and the out-of-plane vibration of the central oxide ion, respectively. ν(Fe–N) is tentatively assigned to the stretching mode between Fe and N.

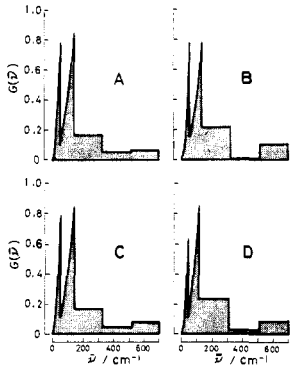

Figure 7. Effective frequency distributions of the lattice vibrations determined by the least-squares method (see the text).

localized phase. This fact implies that we may represent the normal heat capacity by a single smooth curve without any discontinuity at each phase-transition point.

The normal heat capacity of a solid reflects both the continuous phonon distribution and many discrete intramolecular vibrational modes. A borderline between them was assumed in this paper to be located at 700 cm^{-1}. Since the present compound consists of 90 atoms, the number of degrees of freedom for a formula unit is 270. Among them, 20 modes of intramolecular vibration above 700 cm^{-1} (158 degrees of freedom) were reasonably assigned on the basis of the IR spectra. Contribution of these modes to the normal heat capacity was calculated according to the Einstein model. The contribution from the remaining degrees of freedom was effectively included in a continuous spectrum. By using $75C_p$ values in the range 12–85 and 220–300 K or $71C_p$ values in the range 12–85 and 240–300 K, the "best" four effective frequency distributions below 700 cm^{-1} were determined by the least-squares method. The four frequency distributions thus obtained are labeled A, B, C, and D and are illustrated in Figure 7. The normal heat capacities at rounded temperatures are listed in Table II. The present methods reproduced the experimental C_p values within a root-mean-squares deviation of ±0.97 J K^{-1} mol^{-1} or better over the fitting temperature regions. A broken line in Figure 1 represents the normal heat capacity due to the distribution A and the 158 intramolecular vibrations.

The difference between the observed and normal heat capacities corresponds to the excess heat capacity, ΔC_p, due to the phase transitions. In Figure 8, ΔC_p is plotted as a function of temperature. The enthalpy ($\Delta_{trs}H$) and entropy ($\Delta_{trs}S$) arising from the phase transitions were determined by integration of ΔC_p with respect to T and ln T, respectively. The variation in $\Delta_{trs}S$ with different normal heat capacities is small. The average value is $\Delta_{trs}S$ = (30.58 ± 0.83) J K^{-1} mol^{-1} (see Table II). Table III lists $\Delta_{trs}H$ and $\Delta_{trs}S$ estimated on the basis of distribution A.

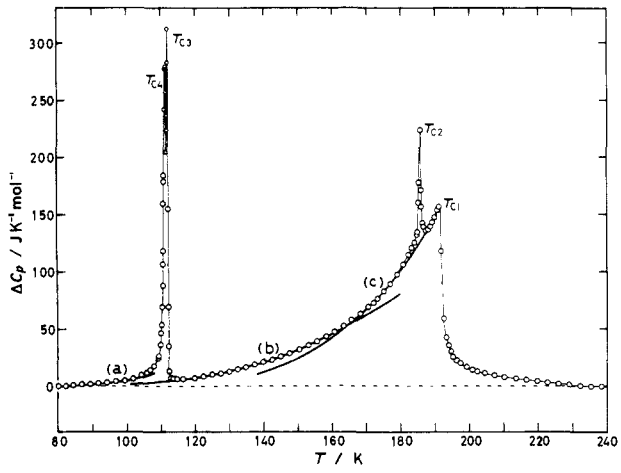

Figure 8. Excess heat capacity, ΔC_p, due to the phase transitions of $[Fe_3O(OAc)_6(py)_3](py)$. Thick lines labeled (a), (b), and (c) represent the calculated values from eq 1.

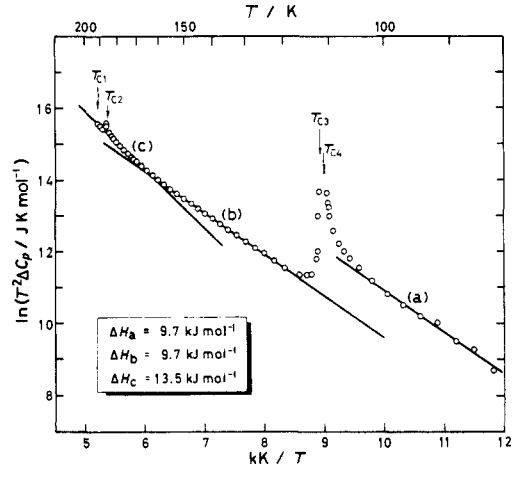

Figure 9. Plot of ln ($T^2\Delta C_p$) (J K^{-1} mol^{-1}) against $1000K/T$.

As revealed by Mössbauer spectroscopy[10,11] and the present heat capacity measurements, the intramolecular electron transfer takes place over a wide temperature region. This situation is obviously reflected in the long tail of ΔC_p shown in Figure 8. Interestingly, ΔC_p was found to be reproduced by the simple equation

$$\Delta C_p = \left(\frac{A}{T^2}\right) \exp(-B/T) \tag{1}$$

This has the same form as that initially derived for the excess heat capacity due to vacancy formation.[18] If a vacancy formation is replaced by an excitation due to the intramolecular electron transfer, we can discuss the present phase transition based on this equation. When the enthalpy gain required for the intramolecular electron transfer is ΔH, ΔC_p is written by a form

$$\Delta C_p = \left(\frac{\partial \Delta H}{\partial T}\right)_p = \left(\frac{\partial nh}{\partial T}\right)_p \tag{2}$$

where n, the number of excited molecules, is given by

$$n = N_A \exp\left(\frac{s}{k}\right) \exp\left(-\frac{h}{kT}\right) \tag{3}$$

(18) Lidiard, A. B. *Handb. Phys.* **1957**, *20* (Part 2), 246.

Table I. Molar Heat Capacity of $[Fe_3O(CH_3CO_2)_6(C_5H_5N)_3](C_5H_5N)$: Relative Molecular Mass = 854.214

T, K	C_p, J K^{-1} mol^{-1}	T, K	C_p, J K^{-1} mol^{-1}	T, K	C_p, J K^{-1} mol^{-1}	T, K	C_p, J K^{-1} mol^{-1}
Series 1		185.459	868.81	Series 2		Series 3	
82.375	425.38	186.095	863.72	12.210	31.157	109.284	539.54
84.615	434.58	186.743	832.95	12.918	35.654	109.839	551.51
86.923	443.61	187.397	831.00	13.696	40.087	110.296	569.96
89.351	452.54	188.051	832.92	14.691	45.771	110.653	604.93
91.827	462.08	188.704	837.38	15.766	51.684	110.997	678.26
94.338	470.89	189.355	842.28	16.743	57.956	111.319	797.10
96.880	480.09	190.003	849.02	17.744	63.729	111.632	757.40
99.458	489.43	190.649	855.67	18.820	70.297	111.944	804.09
102.042	499.23	191.293	859.78	19.878	76.700	112.275	591.09
104.402	508.98	191.942	822.64	20.840	82.690	112.636	533.65
105.995	516.24	192.608	764.77	21.726	88.335	113.004	531.13
107.029	521.57	193.287	749.75	22.615	94.055		
108.055	527.77	193.970	744.26	23.510	99.971	Series 4	
109.071	537.68	194.654	740.67	24.480	106.26	110.834	624.39
110.070	562.47	195.339	737.10	25.549	113.33	111.085	697.46
111.010	702.75	196.368	736.35	26.612	120.31	111.243	761.49
111.893	732.00	197.742	736.55	27.673	127.27	111.396	799.19
112.829	534.26	199.422	736.94	28.738	134.38	111.549	777.79
113.827	533.22	200.859	737.23	29.699	140.85	111.704	724.00
114.772	535.56	202.337	739.12	31.065	150.10	111.862	744.85
116.464	540.13	204.512	742.17	32.607	160.43	112.014	833.45
119.947	550.17	207.288	746.05	34.080	170.23	112.169	677.06
122.457	558.08	210.447	750.84	35.498	179.75	112.340	556.85
125.013	566.19	213.591	755.89	36.864	188.77	112.519	536.01
127.539	573.51	216.719	761.25	38.208	197.43		
130.036	581.40	219.831	766.47	39.572	206.27	Series 5	
132.506	589.51	222.928	771.90	41.201	216.55	110.363	568.99
134.985	597.20	226.035	776.94	43.053	228.21	110.517	586.30
137.474	605.36	229.150	782.95	44.849	239.54	110.691	604.68
139.990	613.36	232.276	788.40	46.579	250.44	110.862	636.26
142.534	621.53	235.437	794.18	48.427	261.82		
145.077	629.89	238.609	800.50	50.371	273.29	Series 6	
147.652	638.77	241.766	806.90	52.259	284.74	184.988	824.67
150.364	647.89	244.934	813.36	54.177	295.34	185.379	851.52
153.071	657.51	248.115	819.66	56.061	305.53	185.759	915.54
155.642	666.71	251.975	826.68	57.857	314.99	186.138	848.96
158.189	676.51	254.771	833.02	59.678	324.84	186.526	835.63
160.720	686.12	257.954	839.26	61.717	335.15		
163.235	696.28	261.121	845.57	63.730	344.77		
165.727	706.98	264.273	852.65	65.744	354.65		
168.196	717.97	267.409	859.12	67.771	363.76		
170.641	729.28	270.530	866.67	69.799	373.0,		
172.100	735.70	273.635	874.65	71.831	382.34		
173.207	741.73	276.726	880.01	73.872	391.48		
175.006	751.76	279.805	886.34	75.923	399.87		
176.993	762.68	282.871	892.19	77.986	408.54		
178.965	774.53	285.924	898.52	80.064	416.69		
180.918	787.78	288.961	905.30				
182.373	799.43	291.981	913.64				
183.335	807.44	294.986	920.21				
184.147	814.30	297.983	925.33				
184.808	821.89	300.971	930.63				

N_A is Avogadro's constant, k is the Boltzmann constant, and h and s are the enthalpy and entropy necessary for the excitation of a single molecule. By substituting eq 3 for n in eq 2, we obtain the form of eq 1. It is obvious that a plot of ln $(T^2\Delta C_p)$ against $1/T$ gives a straight line, whose slope is $-h/k$ (see Figure 9). There are three temperature regions in which ΔC_p is represented by a single formula: region (a) below 100 K, region (b) 120–165 K, and region (c) 165–190 K except for the transition region of T_{C2}. The corresponding ΔC_p curves are drawn in Figure 8 as thick lines labeled a, b, and c. The excitation enthalpy in each temperature region was found to be $\Delta H_a = 9.7$, $\Delta H_b = 9.7$, and $\Delta H_c = 13.5$ kJ mol^{-1}.

Since a phase transition is a cooperative phenomenon, the present treatment assuming a temperature-independent excitation enthalpy is, of course, too simple a model. However, a discussion of ΔH at least at the initial stage of a phase transition, say regions (a) and (b), seems to be meaningful. It is instructive to consider a fully ordered crystal at low enough temperatures, where the isosceles triangles formed by the $Fe^{III}{}_aFe^{II}{}_bFe^{III}{}_c$-triad are regularly oriented throughout a crystallite. If the extra d electron on the Fe^{II} ion in a given triad transfers to one of the adjacent iron(III) positions in the same triad, this will result in a state with a higher energy by ΔH(intra). The changed form of the complex after electron transfer, for example, $Fe^{III}{}_aFe^{III}{}_bFe^{II}{}_c$, would immediately influence the intermolecular interaction with six nearest-neighbor Fe_3O complexes through the pyridine ligands, for X-ray structural work[13] has revealed appreciable π–π overlap between the pyridine ligands of neighboring Fe_3O complexes. Thereby, the intermolecular interaction energy would be increased by ΔH(inter) in comparison with that in the otherwise perfectly ordered state. At the same time, the energy state of the pyridine solvate molecules around the given triad would be altered by ΔH(solvate) mainly through a change in its orientational mode. In other words, ΔH consists of a sum of ΔH(intra), ΔH(inter), and ΔH(solvate). Based on variable-temperature Mössbauer spectra, Dziobkowski et al.[19] have estimated an activation energy of $\Delta E^* = 5.6$ kJ mol^{-1} for the thermal electron-transfer barrier in $[Fe_3O(OAc)_6(H_2O)_3]$.

(19) Dziobkowski, C. T.; Wrobleski, J. T.; Brown, D. B. *Inorg. Chem.* **1981**, *20*, 679.

Table II. Normal Heat Capacity and the Transition Entropy

	spectrum				
	A	B	C	D	
temp region for fitting, K	12–85 220–300	12–85 220–300	12–90 240–300	12–90 240–300	
root mean sq. of ΔC_p	±0.93	±0.97	±0.74	±0.96	
T, K	C_p(normal), J K^{-1} mol^{-1}				C_p(obsd), J K^{-1} mol^{-1}
		Fitting Region			
20	77.57	77.78	77.57	76.67	77.46
40	209.48	208.95	209.45	210.23	208.97
60	326.25	325.71	326.43	325.54	326.47
80	416.11	417.47	416.25	416.30	416.44
240	804.07	803.37	803.20	803.77	803.32
260	845.42	845.23	844.95	845.14	843.34
280	886.66	887.07	886.61	886.47	886.72
300	927.59	928.65	927.95	927.53	928.91
		Interpolated Region			
90	453.14	455.11	453.09	453.99	455.04
100	486.16	488.28	485.85	487.45	491.49
110	515.92	517.99	515.30	517.47	558.02
120	543.25	544.92	542.34	544.78	550.34
130	568.63	569.78	567.44	570.01	581.29
140	592.53	593.12	591.12	593.69	613.39
150	615.33	615.40	613.76	616.24	646.66
160	637.34	636.96	635.67	638.00	683.39
170	658.79	658.06	657.09	659.22	726.32
180	679.88	678.90	678.19	680.10	781.55
190	700.74	699.60	699.10	700.79	848.99
200	721.46	720.27	719.93	721.38	737.06
210	742.12	740.96	740.72	741.94	750.16
220	762.76	761.70	761.52	762.51	766.76
230	783.41	782.50	782.34	783.12	784.43
$\Delta_{trs}S$, J K^{-1} mol^{-1}	30.65	30.12	31.71	29.83	
	$\Delta_{trs}S$(av), J K^{-1} mol^{-1} = 30.58 ± 0.83				

Table III. Enthalpy and Entropy of the Phase Transitions in $[Fe_3O(OAc)_6(Py)_3](Py)$

transition	T_C, K	$\Delta_{trs}H$, J mol^{-1}	$\Delta_{trs}S$, J K^{-1} mol^{-1}
T_{C4} T_{C3}	111.4 112.0	503	4.61
T_{C2} T_{C1}	185.8 191.5	4440	26.04
total		4943	30.65

ΔE^* is not a quantity that can be compared directly with the present excitation enthalpy, say, ΔH_a or ΔH_b. However, in view of the fact that ΔH(intra) should be smaller than ΔE^*, it is possible to say that the contributions from ΔH(inter) and ΔH(solvate) are relatively large for the phase transitions of $[Fe_3O(OAc)_6(py)_3](py)$.

Nature of Phase Transitions

Transition entropy, $\Delta_{trs}S$, plays a diagnostic role in the elucidation of the nature of phase transition. As shown in Figure 10, $\Delta_{trs}S$ for $[Fe_3O(OAc)_6(py)_3](py)$ approaches a value of $\sim R$ ln 2 at the transitions of T_{C4} and T_{C3}, where R is the gas constant. With a further increase in sample temperature, $\Delta_{trs}S$ gradually increases to become (30.58 ± 0.83) J K^{-1} mol^{-1} at temperatures far above T_{C1}. Based on this total value of the transition entropy, it is possible to discuss what kinds of degrees of freedom could contribute to the phase transitions in this mixed-valence complex. From Mössbauer results,[10,11] it is clear that in $[Fe_3O(OAc)_6(py)_3](py)$, the transformation from a localized to a delocalized electronic structure occurs over the range ~112–190 K. This correlates well with the long C_p tail spreading over ~115–190 K and culminating in a peak at T_{C1} = 191.5 K. The single-crystal X-ray diffraction results[13] indicate that the C_3 axis disappears at ~190 K as the crystal is cooled from 300 K. This, together with the DTA data for the solid solutions, indicates that the onset of the rotation of the pyridine solvate molecules is seen at T_{C2} = 185.8 K.

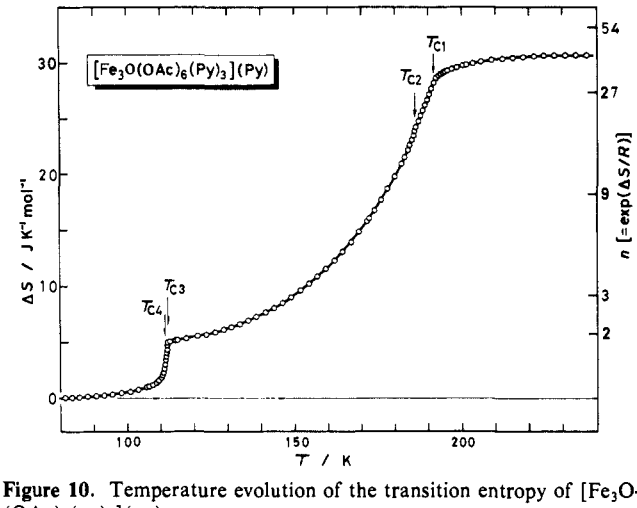

Figure 10. Temperature evolution of the transition entropy of $[Fe_3O(OAc)_6(py)_3](py)$.

The contribution to the transition entropy from the onset of rapid intramolecular electron transfer in $[Fe_3O(OAc)_6(py)_3](py)$ is obviously R ln 3 (=9.13 J K^{-1} mol^{-1}). The entropy due to orientational disordering of the pyridine solvate molecules about the C_3 axis is also R ln 3. As described in the previous section, the present compound does not appear to show any appreciable changes in the molecular vibrational frequencies on going through each phase-transition point. Therefore, the contribution from the phonon system, if any, seems to be negligibly small. The sum of the above contributions amounts of R ln 9 (=18.27 J K^{-1} mol^{-1}), which is only 60% of the observed value. We shall discuss the following two possibilities which seem to be responsible for the remaining transition entropy: either a contribution from a change in the orbital degeneracy of the Fe^{II} ion or a contribution from the rotation of the pyridine solvate molecule about its pseudo-C_6 axis.

The high-spin Fe^{II} in an octahedral ligand field (O_h) is triply degenerate ($^5T_{2g}$). This orbital degeneracy is partially lifted in a lower symmetry field to give a nondegenerate ground level of $^5B_2$ or $^5A_1$ under D_{4h} or C_3 symmetry, respectively. According to the X-ray structural analysis,[13] the Fe_3 triad of such a mixed-valence iron acetate complex forms a fairly distorted isosceles triangle in the lowest-temperature electron-localized phase, whereas it becomes equilateral in the highest-temperature electron-delocalized phase. Therefore, if the site symmetry around the Fe^{II} ion is high in the electron-delocalized phase and low in the localized phase, we can expect an additional entropy gain of R ln 3 arising from the degenerate orbital of the Fe^{II} ion. If this is the case, the total entropy change amounts to 27.40 J K^{-1} mol^{-1} ($=3R$ ln 3). This value is close to the experimental value of 30.58 J K^{-1} mol^{-1} and the small difference (3.18 J K^{-1} mol^{-1}) between them might be due to a phonon contribution neglected above and the uncertainty involved in the estimate of "normal" heat capacity. It should be remarked that the present argument will be valid even when the site symmetry is not exactly O_h symmetry in the highest-temperature phase unless the level splitting of $^5T_{2g}$ under a lower symmetry far exceeds the thermal energy of kT.

The second possibility is derived from a comparison with $[Fe_3O(OAc)_6(4\text{-Me-py})_3](C_6D_6)$, where 4-Me-py is 4-methylpyridine and the solvate molecule is a deuterated benzene. This compound is isostructural with $[Fe_3O(OAc)_6(py)_3](py)$ and shows a similar temperature dependence in its Mössbauer spectrum. A complete single-crystal ^2H NMR study[14] carried out at room temperature clearly shows that the C_6D_6 molecule is rapidly rotating not only about the 6-fold axis but also about the crystallographic C_3 axis along the molecular stacks. If this type of rotation of the pyridine solvate molecule about a pseudo-6-fold axis occurs in $[Fe_3O(OAc)_6(py)_3](py)$, an entropy gain of R ln 6 is expected because pyridine is a six-membered heterocyclic molecule. With electronic delocalization and rotation of the pyridine solvate molecules about both the C_3 and pseudo-C_6 axes, the total entropy of the phase transitions amounts to 33.17 J K^{-1} mol^{-1} ($=2R$ ln $3 + R$ ln 6). This value can also well account for the experimental value of 30.58 J K^{-1} mol^{-1}. We have at present no definitive evidence as to which possibility is responsible for the excess transition entropy beyond the contributions from the intramolecular electron transfer and the orientational disorder of the pyridine solvate molecules about the C_3 axis. It is, however, obviously true that the present thermodynamic study revealed the necessity of introduction of new freedom other than those so far taken into account to interpret correctly the present phase-transition phenomenon.

The nature of the low-temperature-phase transitions at 111.4 and 112.0 K has not been elucidated in this paper. In a later paper,[20] a proposal will be made for these transitions, and a general theoretical model will be advanced to account for phase transitions in these mixed-valence Fe_3O acetate complexes.

(20) Kambara, T.; Sorai, M.; Oh, S. M.; Hendrickson, D. N., unpublished results.

Conclusions and Comments

Heat capacity results have been used to demonstrate the presence of several phase transitions in the mixed-valence compound $[Fe_3O(O_2CCH_3)_6(py)_3](py)$. One of the phase transitions has a long C_p tail spreading over the ~115–190 K range. From Mössbauer measurements, it is clear that this phase transition involves a transformation of the mixed-valence Fe_3O complexes from an electronically localized to an electronically delocalized state. It appears that this transformation is facilitated by the onset of rotation of the pyridine solvate molecules about the C_3 axes that run down the stacks of Fe_3O molecules. As we have indicated in previous papers,[10,11,14] there is an environmental control of the rate of *intra*molecular electron transfer in these mixed-valence complexes. It is likely that the onset of rotation of the pyridine solvate molecules is necessary in order to modify the potential energy diagram for a single Fe_3O complex. The potential energy barrier for *intra*molecular electron transfer is affected by the onset of rotation of the pyridine solvate molecules. Only when the solvate molecules are rotating rapidly does a given Fe_3O complex have a C_3 site symmetry. The analogous mixed-valence complex where this solvate molecule has been removed, i.e., $[Fe_3O(O_2CCH_3)_6(py)_3]$, has been shown[10,11] to be localized on the Mössbauer time scale from liquid helium up to room temperature.

An overview of recent results on the environmental control in the solid state of the rate of *intra*molecular electron transfer for mixed-valence complexes has appeared.[21] Phase transitions are involved not only in several mixed-valence iron acetate complexes but also in mixed-valence biferrocenes.[22] The onset of motion in solvate molecules, ligands, and counterions plays a crucial role in determining the rate of *intra*molecular electron transfer. It is also possible that similar environmental controls on the rate of electron transfer occur in biological electron transport chains. In these transport chains, electron transfer occurs over large distances between two redox sites, each embedded in separate protein structure. The redox potentials of the two sites differ by a small value, and in essence the pair of sites comprise a mixed-valence complex. It is quite possible that certain amino acid residues that made up a given "pathway" for electron transfer are involved in motion under physiological conditions. This motion could be modulating the rate of electron transfer.

Acknowledgment. One of the authors (M. S.) wishes to express his sincere thanks to the Ministry of Education, Science and Culture for a Grant-in-Aid for Scientific Research. D.N.H. is grateful for funding from National Institutes of Health Grant HL16352.

(21) Hendrickson, D. N.; Oh, S. M.; Dong, T.-Y.; Kambara, T.; Cohn, M. J.; Moore, M. F. *Comments Inorg. Chem.*, in press.

(22) (a) Dong, T.-Y.; Cohn, M. J.; Hendrickson, D. N.; Pierpont, C. G. *J. Am. Chem. Soc.* **1985**, *107*, 4777. (b) Cohn, M. J.; Dong, T.-Y.; Hendrickson, D. N.; Geib, S. J.; Rheingold, A. L. *J. Chem. Soc., Chem. Commun.* **1985**, 1095. (c) Dong, T.-Y.; Hendrickson, D. N.; Iwai K.; Cohn, M. J.; Geib, S. J.; Rheingold, A. L.; Sano, H.; Motoyama, I.; Nakashima, S. *J. Am. Chem. Soc.*, in press. (d) Dong, T.-Y.; Hendrickson, D. N.; Pierpont, C. G.; Moore, M. F. *J. Am. Chem. Soc.*, in press.